# Inferring flow energy, space and time scales: freely-drifting vs fixed point observations

Aurelien Luigi Serge Ponte[1], Lachlan Astfalck[2,3], Matthew Rayson[2], Andrew Zulberti[2], and Nicole Jones[2]

[1]Ifremer, Université de Brest, CNRS, IRD, Laboratoire d'Océanographie Physique et Spatiale, IUEM, Brest, France
[2]Oceans' Graduate School, The University of Western Australia, Crawley, Australia
[3]School of Physics, Mathematics and Computing, The University of Western Australia, Crawley, Australia

**Correspondence:** Aurélien Ponte (aurelien.ponte@ifremer.fr)

**Abstract.** A novel method for the inference of spatiotemporal decomposition of oceanic variability is presented and its performance assessed in a synthetic idealized configuration. The method is designed here to ingest velocity observation. The abilities of networks of reduced number of surface drifters and moorings at inferring spatiotemporal scales of ocean variability are quantified and contrasted. The sensitivities of inference performances for both types of platforms to the number of observation,

5 geometrical configurations, flow regimes are presented. Because they simultaneously sample spatial and temporal variability, drifters are shown to be able to capture both spatial and temporal flow properties even when deployed in isolation. Moorings are particularly adequate for the characterization of the flow temporal variability, and may also capture spatial scales provided they are multiplied and the financial and environmental costs of associated deployments can be assumed. We show in particular that the method correctly identifies whether drifters are sampling preferentially spatial vs temporal variability. This method

10 opens novel avenues for the analysis of existing datasets as well as the design of future experimental campaigns targeting the characterization of small scale (e.g. <100 km) Ocean variability.

## 1 Introduction

Characterizing oceanic surface motions in terms of their spatial and temporal scales is a recognized pathway toward the identification of the numerous processes that occur in the Ocean as well as toward an improved understanding of their occurrences,

15 life cycle, interactions and impact on other components of the Ocean variability (Ferrari and Wunsch, 2009). Arbic et al. (2014) critically relied on horizontal wavenumber-frequency decompositions in order to quantify and rationalize the impact of ocean mesoscale turbulence on longer ocean variability in idealized, realistic numerical simulations and altimetric observations. At higher frequencies, wavenumber-frequency decompositions enable the separation of internal gravity waves and balanced motions which share similar spatial scales and are therefore entangled in instantaneous two-dimensional data sources (Torres

20 et al., 2019; Jones et al., 2023). Thanks to wavenumber-frequency decompositions, Qiu et al. (2018) were able to quantify the so-called 'transition scale' above which altimetric observations are dominated by balanced turbulence and below which smaller scales are dominated by internal gravity waves. These decompositions are easily performed with numerical simulations outputs which are provided on a regular spatial and temporal grid and complete. But the lack of observational knowledge of the

high frequency and small scale distribution of energy is a recognized limitation for the validation of tide resolving kilometer
25 resolution global or bassin scale numerical models of the ocean circulation (Arbic et al., 2018; Yu et al., 2019b; Arbic et al.,
2022).

The characterization of ocean variability in terms of spatial and temporal scales is also relevant for operational perspectives. The description one variable's autocorrelation properties is indeed a prerequisite information for the mapping of sparse observations via optimal interpolation (Bretherton et al., 1976; Bretherton and McWilliams, 1980). Ocean surface currents
30 estimations heavily rely for instance on the accurate mapping of altimetric observations which consists in narrow (order 5 to 10 km) geographically and temporally distant tracks (Pujol et al., 2016). The upcoming of wide swath altimetric (Morrow et al., 2019) and current measuring satellite missions introduced novel challenges regarding the mapping of the variables observed and the separation of slower balanced motions and faster internal gravity waves and motivated the development of novel strategies for the separation of the signatures associated to both class of motions. These strategies rely on *a-priori* knowledge of the
35 motions' spatial and temporal scales (Barth et al., 2014, 2021; Ubelmann et al., 2021, 2022).

The in situ characterization of ocean variability at small mesoscales and submesoscales (e.g. <100 km, <10 days) has been a central objective for a number of ambitious experimental efforts over the last decade: LatMIX (Shcherbina et al., 2015); Carthe Consortium (Poje et al., 2014; D'Asaro et al., 2018); OSMOSIS (Buckingham et al., 2016; Yu et al., 2019a); SMODE (Farrar et al., 2020). Dense dedicated mooring deployments of OSMOSIS have for instance shed light on the time-space decomposition
40 of upper ocean variability and highlighted in particular difficulties associated with the Doppler shifting of small-scale structures when observed from fixed platforms (Callies et al., 2020). These experiments represent important financial and environmental efforts however any optimization in the experimental design and/or improved data analysis strategies should be welcome. The present study intends to highlight the fact that drifters represent cheap and experimentally light platforms for the space-time scale characterization of ocean variability provided adequate methodological progresses are obtained. The study presents one
45 such methodological development.

The characterization of oceanic motions in terms of horizontal spatial scales and temporal scales from observations represents a challenge in general that depends on the class of motions of interest, the quantity and nature of observations available, and, the lack of generic metholodology. Fixed point platforms provide information that is horizontally localized over a potentially extended time periods and with temporal fine resolution. Such data are naturally adapted to a decomposition in terms
50 of temporal scales (Polzin and Lvov, 2011). The tracking of surface and subsurface drifting platforms provide ocean current observations which are also amenable to temporal decompositions (Lumpkin et al., 2017). At multi-daily to monthly time scales, drifters have enabled characterizations of mesoscale eddy variability via inspection of surface current autocorrelation or spectral properties (Zhang et al., 2001; Lumpkin et al., 2002; Veneziani et al., 2004; Sykulski et al., 2016) or rotary wavelet decompositions (Lilly and Gascard, 2006; Lilly et al., 2011). The Global Drifter Program has over ∼30 years enabled the col-
55 lection of surface current information worldwide. Recently, the advent of GPS and wider bandwidth satellite communications opened the door to high frequency sampling of surface drifter positions and the generation of surface drifter velocity datasets with global hourly coverage (Elipot et al., 2016). Over the last decade, global descriptions of the Ocean surface high frequency variability have emerged (Elipot et al., 2010, 2016; Yu et al., 2019b; Arbic et al., 2022). These descriptions are timely to vali-

date kilometer scale tide-resolving basin scale numerical simulations that have also emerged over the last decade (Arbic et al., 2018).

Satellite observations are in general well designed to characterize surface spatial variability. The constellation of conventional nadir altimeters provide maps of sea level and surface currents which resolve larger mesoscale motions (Ballarotta et al., 2019). Spatial and temporal gaps between nadir altimeters presumably impose the effective spatial and temporal resolutions of the product which are weakly sensitive to the combination with drifter data or more advance methodology (Ballarotta et al., 2022). Amongst the same range of scales, there are, as a consequence, multiple characterizations of ocean variability in terms of its spatial and temporal scales which in general combine altimetry with other in situ datasets, e.g. moorings, XBTs, tomography (Zang and Wunsch, 2001; Wunsch, 2010; Wortham and Wunsch, 2014). At smaller spatial scales, ship based measurement of tracers and currents have informed about the spatial scales of ocean variability (Callies and Ferrari, 2013) but such measurements potentially entangle spatial and temporal contributions to an unclear extent. Drifters are thought to offer promising perspectives for the description of smaller mesoscale and submesoscale variability (Balwada et al., 2016, 2021). Dedicated experiments with deployments of large number of surface drifters such as that conducted by the Carthe Consortium have provided useful datasets to demonstrate this despite also highlighting potential biases associated the horizontal divergent character of the flow at these scales (Poje et al., 2017; Pearson et al., 2019, 2020; Wang and Bühler, 2021).

This work considers an idealized configuration of ocean variability whose properties and synthetic generation are described in Section 2.1. A novel method for the inference of the flow properties are then described in Section 2.3. The inference is then applied in several scenarios of observations in order to explore the performance of inferences to the number of observations (Section 3.2), to platform spatial separation (Section 3.1), and, to flow regime (Section 3.3). The results are discussed and conclusions drawn in Section 4.

## 2 Method

### 2.1 Flow design

The bidimensional and time variable flow is described by the sum of rotational and divergent contributions and is described as

$$u = -\partial_y \psi + \partial_x \phi, \tag{1}$$
$$v = \partial_x \psi + \partial_y \phi. \tag{2}$$

where $u$ and $v$ are the zonal and meridional velocities, $\psi$ is the streamfunction, $\phi$ is the velocity potential and $\partial_x$ and $\partial_y$ are the partial derivatives in $x$ and $y$, respectively. We can describe the second-order behaviour of $\psi$ and $\phi$, equivalently, by either their covariance functions or spectral densities. For general random fields $a$ and $b$, defined over $\mathbf{x}$, we define the stationary covariance function as $C_{ab}(\mathbf{x}) = \langle a(\mathbf{x}_0), b(\mathbf{x}_0 + \mathbf{x}) \rangle$ where the inner product is given as the covariance inner product $\langle a, b \rangle = \mathrm{E}[(a - \mathrm{E}[a])(b - \mathrm{E}[b])]$. Here, the boldface $\mathbf{x}$ denotes a location in space and time. We define the spectral density as $S_{ab}(\boldsymbol{\omega})$, where the boldface $\boldsymbol{\omega}$ represents a location in wave-number and frequency space. The covariance function and the

spectral density are related via Wiener–Khinchin's Theorem so that

$$C_{ab}(\mathbf{x}) = \frac{1}{2\pi} \int_{-\infty}^{\infty} S_{ab}(\boldsymbol{\omega}) \exp(i\boldsymbol{\omega}\mathbf{x}) \, \mathrm{d}\boldsymbol{\omega}, \quad \text{and} \quad S_{ab}(\boldsymbol{\omega}) = \int_{-\infty}^{\infty} C_{ab}(\mathbf{x}) \exp(-i\boldsymbol{\omega}\mathbf{x}) \, \mathrm{d}\mathbf{x}. \tag{3}$$

Given an assumed parameterisation of $C_{\psi\psi}$, $C_{\phi\phi}$ and $C_{\psi\phi}$ the horizontal velocity auto- and cross-covariances are thus

$$C_{uu} = -\partial_{yy}C_{\psi\psi} - \partial_{xx}C_{\phi\phi} + \partial_{xy}C_{\phi\psi} + \partial_{xy}C_{\psi\phi}, \tag{4}$$

$$C_{vv} = -\partial_{xx}C_{\psi\psi} - \partial_{yy}C_{\phi\phi} - \partial_{xy}C_{\phi\psi} - \partial_{xy}C_{\psi\phi}, \tag{5}$$

$$C_{uv} = \partial_{xy}C_{\psi\psi} - \partial_{xy}C_{\phi\phi} + \partial_{yy}C_{\phi\psi} - \partial_{xx}C_{\phi\psi}. \tag{6}$$

Similarly, given the spectral densities $S_{\psi\psi}$, $S_{\phi\phi}$ and $S_{\psi\phi}$, we define the power and cross-power spectral densities of the horizontal velocities as

$$S_{uu} = l^2 S_{\psi\psi} + k^2 S_{\phi\phi} - kl(S_{\psi\phi} + S_{\phi\psi}), \tag{7}$$

$$S_{vv} = k^2 S_{\psi\psi} + l^2 S_{\phi\phi} + kl(S_{\psi\phi} + S_{\phi\psi}), \tag{8}$$

$$S_{uv} = kl(S_{\phi\phi} - S_{\psi\psi}) - k^2 S_{\psi\phi} + l^2 S_{\phi\psi}. \tag{9}$$

For our numerical experiment, we derive a purely rotational flow by setting $\phi = 0$ and so, simply, $u = -\partial_x\psi$ and $v = \partial_x\psi$. This leads to the covariance functions $C_{uu} = -\partial_{yy}C_{\psi\psi}$, $C_{vv} = -\partial_{xx}C_{\psi\psi}$ and $C_{uv} = \partial_{xy}C_{\psi\psi}$, and spectral densities $S_{uu} = l^2 S_{\psi\psi}$, $S_{vv} = k^2 S_{\psi\psi}$ and $S_{uv} = -kl S_{\psi\psi}$.

To parameterise the flow we seek either a covariance function or spectral density that satisfies physical requirements of the streamfunction $\psi$; namely, we require a log-linear decay in the high-frequency/wavenumber of the spectral density. A good candidate for this is the Matérn covariance function (Lilly et al., 2017) with auto-covariance function and power spectral density

$$C(x) = \frac{2^{1-\nu}\eta^2}{\Gamma(\nu)} |\lambda x|^\nu \mathcal{K}_{|\nu|}(|\lambda x|), \quad \text{and} \quad S(\omega) = \frac{c_\nu \eta^2}{(\omega^2 + \lambda^2)^{\nu+1/2}}, \quad \text{where} \quad c_\nu = \frac{2\pi\lambda^{2\nu}\Gamma(\nu + 1/2)}{\Gamma(1/2)\Gamma(\nu)},$$

$\Gamma(\cdot)$ denotes the Gamma function and $\mathcal{K}_{|\nu|}$ is the modified Bessel function of the second kind of order $\nu$. For positive integer values minus $1/2$ of $\nu$, i.e. $\nu = p - 1/2$ where $p \in \mathbb{N}^+$, $\mathcal{K}_{|\nu|}$ has an analytical expression, otherwise it must be numerically calculated. We assume $\psi$ to follow a separable Matérn process in space and time, so that $C_{\psi\psi}(\mathbf{x}) = C_{ss}(d) \cdot C_{tt}(t)$ where $\mathbf{x} = [d, t]$, $d$ represents isotropic distance, and with parameters $\nu = \nu_s = 2$ and $\lambda_s$ for the kernel defined over space ($C_{ss}(d)$), and $\nu = \nu_t = 1$ and $\lambda_t$ for the kernel defined over time ($C_{tt}(t)$). This separability assumption is a concession on realism which enables to substantially ease the computational cost of the flow generation step and is not expected to affect our evaluation of the inference performance (Wortham and Wunsch, 2014; De Marez et al., 2023). The covariance functions with respect to $u$ and $v$ are thus

$$C_{uu}(\mathbf{x}) = -\eta^2 C_{tt}(t) \cdot \frac{y^2 C_{ss}''(d) + x^2 d^{-1} C_{ss}'(d)}{d^2}, \tag{10}$$

$$C_{vv}(\mathbf{x}) = -\eta^2 C_{tt}(t) \cdot \frac{x^2 C_{ss}''(d) + y^2 d^{-1} C_{ss}'(d)}{d^2}, \tag{11}$$

$$C_{uv}(\mathbf{x}) = \eta^2 C_{tt}(t) \cdot \frac{xy \left(C_{ss}''(d) - d^{-1} C_{ss}'(d)\right)}{d^2}, \tag{12}$$

where primes denote derivatives with respect to horizontal distance $d$.

## 2.2 Flow data generation

The streamfunction is generated over a 1000 km by 1000 km domain with 2 km grid spacing and over 100 days with hourly resolution (Fig 1). The amplitude of the streamfunction $\Psi$ is set such as to lead to flow standard deviation $U$, according to: $\Psi = U\lambda\sqrt{(\nu_s - 1)/\nu_s}$. The reference flow simulation is defined by U=0.1 m/s, $\lambda_s = 100$ km, $\lambda_t = 5$ days (Fig 1). We reparameterize the covariance functions by $\eta = \gamma\lambda_s$, where $\gamma$ has the interpretation of being the amplitude parameter on the horizontal velocity process; as well as interpretability, this has some computational benefits.

The hourly synthetic flow is fed to the Parcels python library configured with Runge-Kutta 4 time-stepping and the default A-grid interpolation scheme in order to produce synthetic drifter trajectories (Delandmeter and van Sebille, 2019). Drifters are released initially at all flow grid points albeit in a 20 km strip around boundaries which amounts to 9216 drifters total for each drifter simulation. Trajectories reaching domain boundaries are de-activated and not advected further in time and discarded from the list of observations that will be used for inference. The fraction of trajectories discarded amount to 52% in the reference configuration. Drifter positions are stored at hourly resolution and velocities estimated from drifter positions with a second order finite differences. Example of such trajectories are shown on Figure 1. The flow amplitude averaged over time and space is about $1.8\%$ larger than that computed from drifters trajectories which reveals small turbophoresis (Freeland et al., 1975).

A non-dimensional parameter characterizing the flow is $\alpha = U\lambda_t/\lambda_s$. This parameters is expected to control how the relative importance of spatial vs temporal variability projection on Lagrangian time series (Middleton, 1985). In the reference scenario, the value of the parameter is about $0.4$ which is in the range of values relevant for the Ocean (Lumpkin et al., 2002). In order to obtain mooring and drifters time series with different $\alpha$ values, the synthetic flow is simply rescaled and new Lagrangian trajectories are simulated with the rescaled flow.
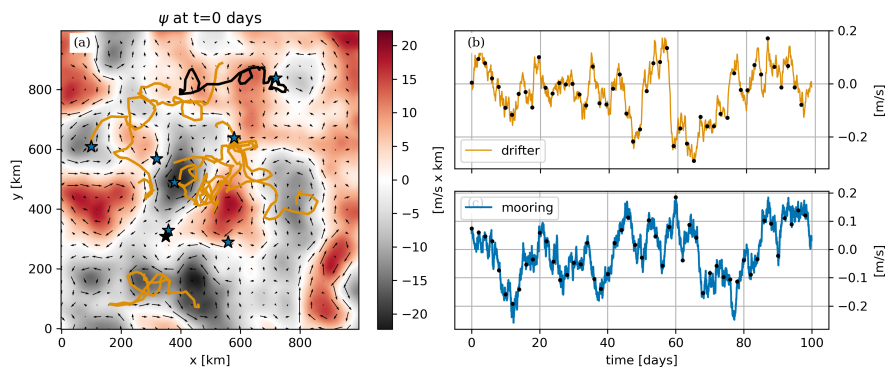
**Figure 1.** Overview of the inference input data for the reference case: (a) streamfunction snapshot in color overlaid with drifters tracks and moorings used for the inference; (b) x velocity time series of drifter identified by the black track on (a); (c) x velocity time series at the mooring indicated by the black star on (a). On (b) and (c), black dots indicate the 2 days sub-sampled data used in the inference.

## 2.3 Inference

Observed data $\mathbf{y}$ is composed of flow time series collected over time by $N_p$ drifters or moorings to which a white noise $\mathbf{n}$ of standard deviation $\sigma$ is added. The critical difference between drifter and mooring observations is that they are collected along drifter trajectories in the former case, i.e. $\mathbf{u}[\mathbf{x}(t)] + \mathbf{n}(t)$ where $\mathbf{x}(t)$ is a drifter trajectory, while they are collected at a fixed location in the latter one, i.e. $\mathbf{u}[\mathbf{x}, t] + \mathbf{n}(t)$ where $\mathbf{x}$ is a mooring location.

We treat the collection of parameters $\Theta = \{\gamma, \lambda_s, \lambda_t, \sigma^2\}$, as uncertain and unknown and probabilistically quantify this uncertainty. We treat $\Theta$ as a random variable and so naturally adopt the Bayesian paradigm of probability. Bayes' Theorem states $\mathrm{p}(\Theta \,|\, \mathbf{y}) \propto \mathrm{p}(\mathbf{y} \,|\, \Theta)\mathrm{p}(\Theta)$, where $\mathrm{p}(\Theta \,|\, \mathbf{y})$ is the posterior distribution, $\mathrm{p}(\mathbf{y} \,|\, \Theta)$ is the likelihood and $\mathrm{p}(\Theta)$ is the prior distribution. The posterior is our target quantity and describes the probability distribution of $\Theta$ conditioned on the observed data. The likelihood is a probability distribution that asses the probability of the data being generated, conditioned on some value of $\Theta$. Finally, the prior represents our knowledge of $\Theta$ before we observe the data $\mathbf{y}$; in this term we may include the results from previous analyses, bounds on values that $\Theta$ may take or any physically derived structure between the constituent parameters inside of $\Theta$. Exact computation of $\mathrm{p}(\Theta \,|\, \mathbf{y})$ is analytically achievable for a small class of model problems; however, this is typically not so and so $\mathrm{p}(\Theta \,|\, \mathbf{y})$ is computed numerically using Markov chain Monte Carlo (MCMC). MCMC can be computationally demanding, and so there are many methodologies for approximating $\mathrm{p}(\Theta \,|\, \mathbf{y})$ without MCMC; such methodologies are designed either to improve computational speed (at the cost of accuracy and exactness in quantifying the probability distribution) or to target a particular aspect of the posterior distribution. For instance, maximum-a-posteriori (MAP) calculates $\arg\max_{\Theta}\{\mathrm{p}(\Theta \,|\, \mathbf{y})\}$, variational Bayesian methods calculate the posterior from an known analytical family that best minimises the Kullback–Leibler divergence, generalised Bayesian inference is a generalisation of this to other divergences, and information theory maximises a metric placed over $\mathrm{p}(\Theta \,|\, \mathbf{y})$, such as entropy. Here, we prefer MCMC so that we may guarantee the accuracy of our results, and note that alternative inference methods may be more suitable in an operational context where larger computational expediency is warranted. MCMC generates a dependent chain of draws from the posterior $\mathrm{p}(\Theta \,|\, \mathbf{y})$ such that subsets of $\Theta$ are visited proportionally to the posterior probability of the subsets. MCMC sampling algorithms are designed so that the sampled draws result in an irreducible Markov chain $\Theta^{[1]}, \ldots, \Theta^{[n]}$ that converges on $\mathrm{p}(\Theta \,|\, \mathbf{y})$ as its stationary distribution. The Markovian property implies that a sample $\Theta^{[i]}$ only depends on its previous sample $\Theta^{[i-1]}$; the method by which $\Theta^{[i]}$ is generated from $\Theta^{[i-1]}$ distinguishes the various MCMC algorithms. All MCMC algorithms propose some $\Theta^{[*]}$ from $\Theta^{[i-1]}$ and with probability $\alpha$ either accept $\Theta^{[*]}$, in which case $\Theta^{[i]} = \Theta^{[*]}$, or reject $\Theta^{[*]}$, in which case $\Theta^{[i]} = \Theta^{[i-1]}$. We generate samples using Metropolis-Hastings (MH), a well-known and accessible MCMC algorithm. Description and particulars are provided in the appendix.

## 2.4 Validation of the Inference Methodology

As the mooring and drifter data are simulated, we know the ground truth, and so may validate the MCMC sampling methodology. We show this for two cases: first, we show the probabilistic parameter estimates from the reference flow (section 2.1); and second, we compare the MAP estimates, i.e. $\hat{\Theta} := \arg\max_{\Theta}\{\mathrm{p}(\Theta \,|\, \mathbf{y})\}$, of an 100-member ensemble with their true values.

Examining a single scenario demonstrates the inherent uncertainty associated with a single experiment; whereas, inference across an ensemble looks at the variability that arises between data-samples. In all cases, the data comprise a bivariate $u$, $v$

175 time-series collected either along 8 trajectories (drifters), or at 8 stationary locations (moorings), with 2 days temporal sampling over 100 days, amounting to 400 data points. The ensemble data are generated from the single spatio-temporal field with randomly sampled drifter tracks and mooring locations. Figure 2 shows the marginal posterior probability distributions of the single-member reference case. For all parameters, the true values lie well within the probability mass. Note, $\sigma^2$ is not well resolved, this is due to the roughness of the Matern process confounding with the noise signal over the sampling interval,

180 and is not alarming. More detailed statistical diagnostics accompany the code in the supplementary material. Figure 3 plots a histogram of the MAP values calculated from each ensemble member's MCMC chain against the true value. This shows the variability of the distributions about the true value over the ensemble. Again, all distributions are centered on the true values, and there exists some difficulty in observing $\sigma^2$ with precision. The precision of the inference will next be quantified by the difference between the third and first quartiles which will be referred to as the inter-quartile width (IQW).
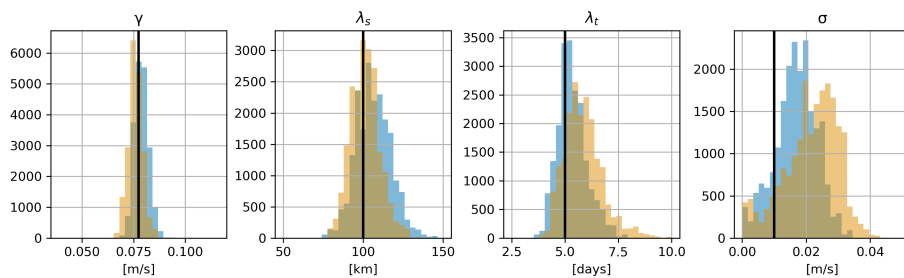
**Figure 2.** Histogram of MCMC samples of single inferences based on 8 drifter trajectories (orange) and 8 mooring locations (blue) observations in the reference case.
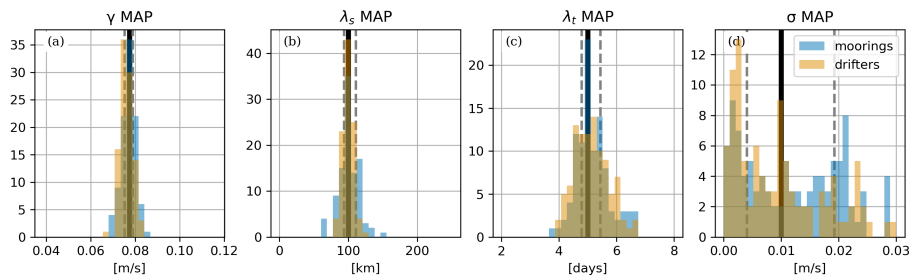
**Figure 3.** Distribution of parameters MAP values for the reference flow and reference observation scenario (scenario REF). True parameters values are represented by vertical black lines. First and third quartiles are grey dashed vertical lines and provide insight into IQW.

185 ## 2.5 Inference scenarios

This study reports on the performance of the inference method under several scenarios (summarized in Table 1):

**Table 1.** Inference scenarios. All other parameters are held constant across scenarios.

| scenario | $\gamma$ [m/s] | $N_p$ | drifters | moorings |
|---|---|---|---|---|
| REF | $7.7 \times 10^{-2}$ | 8 | random draw | random draw |
| SEP[$dx$] | $7.7 \times 10^{-2}$ | 2 | random with initial separation $dx$ | random with separation $dx$ |
| IND[$N_p$] | $7.7 \times 10^{-2}$ | [1-16] | random draw and independent observations | random draw independent observations |
| REG[$\alpha$] | $[1.6 \times 10^{-3} - 4 \times 10^{-1}]$ | 1 | random draw | random draw |

- REF corresponds to the nominal configuration described in Section 2.4 with 8 simultaneously deployed platforms

- SEP[$dx$] - When multiple platforms are simultaneously sampling the flow, the separation between platforms and more generally their geometrical distribution are expected to modulate the performance of the inference. To simplify the analysis, we restrict the configuration to two simultaneous observing platforms and investigate the sensitivity of the inference performance to their separation (with 10% tolerance). For drifters, the separation is the initial one between the two drifters.

- IND - inference is performed by assuming time series from different platforms are independent from each other. Such situation would occur if individual moorings/drifters were deployed at times sufficiently far apart, no correlation could be expected across the velocity time series each recorded. In effect this amounts to quantifying the ability of one platform at capturing flow parameters and investigating the sensitivity to the length of the time series.

- REG[$\alpha$] - the amplitude of the flow is rescaled in order to explore different values of flow regime parameter $\alpha = U\lambda_t/\lambda_s$. The amplitude of the noise is linearly scaled as a function of $\alpha$ in order to maintain a fixed signal to noise ratio. Inference are performed with a single platform.

## 3 Results

### 3.1 Platform separation sensitivity

Under scenario SEP[$dx$], estimations of the flow amplitude are comparable for moorings and drifters observations and precise with IQWs lower than 13% of true amplitudes and no sensitivity to separation (Figure 4a). We argue this follows from the fact that inferences are provided with velocity observations as inputs. Drifter inferences of the flow amplitude exhibit a 1% to 3% low bias which is comparable to that associated with turbophoresis (Section 2.2).

Mooring spatial scale estimates are on the other hand sensitive to separation (Figure 4b). After a modest decrease in performance of the inference as measured by IQWs, best inferences are obtained for separation in the range of 20 and 120 km. For larger separations, the inference precision decreases with IQW reaching values of about 50% of true values at 300 km, i.e. 3 times the flow spatial scale. This loss of performance with separation reflects the loss correlation between the flow measured

by both mooring and thus the lack of information about spatial structure in the dataset. Drifters exhibit no clear sensitivity relatively which may be explained by the substantial displacements of drifters compared to separations considered (864 km over 100 days at $U = 10$ cm/s in straight line) as well as by the natural ability at drifters to explore space and time and therefore constrain spatial scales (see section 3.2).

At separations lower than about 100 km, inferences of the flow temporal scale perform equally for mooring and drifter observations with no bias and IQW of about 37% (Figure 4c). For larger separations, moderate bias emerges and precision decreases with increased IQW (up to about 50%) for both platform types.
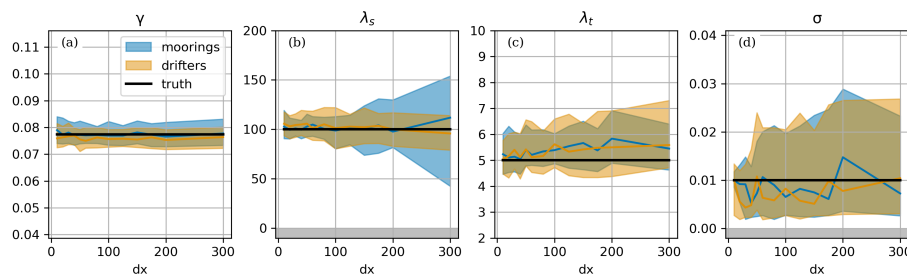
**Figure 4.** Sensitivity of parameters MAP estimates to platform separation (in km) in the 2 platforms configuration (scenario SEP[$dx$]). Lines represent the median, while shaded areas are bounded by first and third quartiles. Truth values are in black. Grey shadings represent the no-go zone of the prior and inference parameter exploration.

### 3.2 Sensitivity of the pseudo single platform inference to time series length

Under scenario IND[$N_p$], single moorings provide estimates of the flow amplitude, $\gamma$, and time scale, $\lambda_t$, parameters that are precise with IQW starting at about 17% and 46% of true values respectively for one platform, and that converge to true values as the number of independent time series is increased (Figure 5). For the maximum number of platforms considered, IQW of flow amplitude and timescale estimates have decreased to 4% and 12% respectively. As expected from their inability to explore the spatial dimension, single moorings are however globally unable to capture the flow spatial scale with IQW comparable to the half the width of the parameter space allowed to be explore, i.e. $[0, 1000\,\mathrm{km}]$, which amounts to the prior uncertainty (that is, there is no resolution of uncertainty).

In comparison, drifters provide estimates of all three flow parameters ($\gamma$, $\lambda_s$, $\lambda_t$) that are precise with IQW starting at about 15%, 86%, 86% for one platform and converge toward truth as the number of platforms is increased with IQW smaller than 17% for all three parameters for 16 platforms. The ability of drifters to capture both spatial and temporal scales is explained by their natural ability at sampling space and time simultaneously. MAP medians indicate mild biases with an underestimation of amplitude and overestimation of time scales which decrease as the number of platform is increased. The amplitude low bias if about 6% with a single drifter and reduces to about $1.4\%$ which is comparable to the turbophoresis bias (Section 2.2).
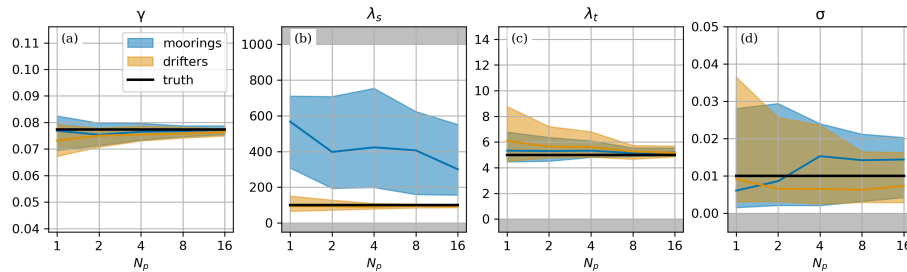
**Figure 5.** Sensitivity of parameters MAP estimates to the number of platforms (scenario IND[$N_p$]). Platforms are assumed independent from each other. Same representation as Figure (4).

### 3.3 Flow regime sensitivity

We turn now to an investigation of the sensitivity of inferences to the flow parameter $\alpha$ (scenario REG[$\alpha$]). We revert to the single platform configuration in order to limit the exchange of information across platforms and the resulting constraint it brings for inference which may mask the $\alpha$ sensitivity. For comparison purposes we also perform a "time-only" inference of drifters velocity time series which estimate flow amplitude and temporal scale and noise, thereby ignoring spatial field decorrelations.

As anticipated from section 3.2, inferences of flow amplitude and time scale from mooring observation are relatively accurate with IQW of about 15% and 50% of true values relatively (Figure 6a-6c). The amplitude inference reflects the linear sensitivity to $\alpha$. Spatial scales remain undetermined no matter $\alpha$ values (Figure 6b). This lack of sensitivity is expected as the nature of mooring observations, that their exclusive sampling of the temporal variability, is not affected by variations of $\alpha$.

Inferences of flow amplitude from drifter observations are comparable to mooring inferences in terms of IQW albeit for a low bias of about 2 to 7%. A comparable bias is observed on time-only inferences for small $\alpha$ values but is exacerbated for $\alpha$ larger than unity and reach about 35% of the true amplitude. For large $\alpha$, distortions of the temporal spectrum shape is likely affecting the overall performance of the time-only inferences which relies on the spectral distribution following that of a Matérn 1 process.

At small $\alpha$ values ($< 0.2$), inferences of the flow spatial scale from drifter observations are worst and nearly comparable to those from mooring observations. Drifters indeed merely moves over a flow timescale compared to the spatial decorrelation scale in this flow regime which has been historically coined "fixed-float" and can be effectively considered as a mooring (Middleton, 1985; Lumpkin et al., 2002). Flow temporal estimates from drifter observations are therefore of comparable performance to estimates from mooring observations.

At larger values of $\alpha$ (e.g. $> 0.2$), the precision of the flow spatial scale inference from drifter observations improves substantially with decreasing IQW (down to 50% at $\alpha \sim 1$). Estimates of the temporal scale deteriorate on the other hand with bias high of about 40% and IQW width of about 100%. At these values, the flow is in the so called "frozen turbulence" regime and drifters are in effect experiencing the spatial variability of the flow field (Middleton, 1985; Lumpkin et al., 2002). This is directly reflected in the estimate of the temporal scale obtained from the "time-only" inference which monotonically decreases

255 with $\alpha$. The fact that the temporal scale from the space-time inference does not follow a similar trend is a testimony to the relevance of the latter method which is able to identify that observations reflect a predominance of spatial variability and attribute reasonable space and time scale estimates, albeit with moderate error and bias.
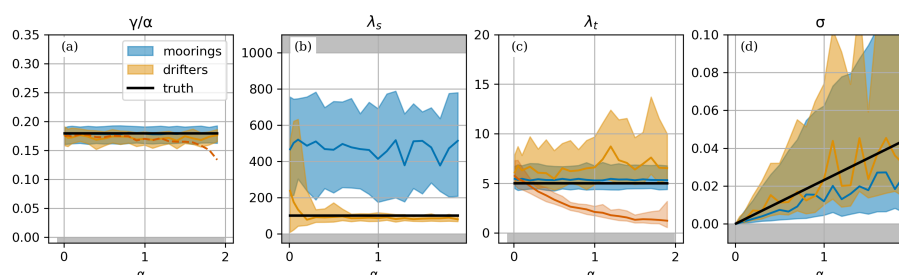
**Figure 6.** Sensitivity of parameters MAP estimates to flow regime $\alpha$ in the single platform configuration (scenario REG[$\alpha$]). Time only drifter inference is in red on (b) (median MAP dashed) and (d) (quartiles and median). Same representation as Figure (4) otherwise.

## 4 Conclusions

We have presented a novel Bayesian method to infer ocean circulation spectral parameters (e.g. amplitude, space and time

260 scales) from sparse observations of the flow. The intention here was to quantify parameter uncertainty due to sampling and flow regimes. These results may guide future field and analysis campaigns and open novel avenues for the analysis of existing datasets. We considered flow observation from two type of platforms typically employed in Oceanography: moorings which provide fixed point flow observations and drifters that provide along-flow flow observations. Inferences based on both types of platforms provide estimates that converge to true values as the number of observations is increased. The performance of

265 the method was quantified in various observing configurations which allowed to highlight pros/cons of each type of platform. As already recognized, moorings are well suited to characterize temporal scales of variability and can if deployed simultaneously enable to constrain flow spatial scales. Drifters naturally sample both space and time and we showed they enable to simultaneously constrain the flow space and time scales even when developed in isolation which is a first time demonstration to our knowledge. A flow parameter quantifying displacements of drifters relative to space and time scales modulated the

270 ability of drifter at characterizing flow properties. Given the relative low cost and low environmental impact associated with drifter deployments compared to moorings, we argue they provide a powerful and more sustainable mean to characterize flow properties.

More developments are required in order to make this method applicable to realistic oceanographic configurations. First the method needs to be extended to flows that are composed of a superposition of processes commonly occurring in the Ocean,

275 e.g. internal waves and tides, near-inertial waves. Such extension will present methodological challenges associated with the parametrization of the space/time variability associated with these processes. The assumption of space/time separability, which was imposed here by the selected method of flow field generation, may have to be relaxed in a realistic configuration (Wortham
and Wunsch, 2014; De Marez et al., 2023). As long as correlations may be expressed in physical space, extension of the inference to non-separable cases is direct. It may also be useful to generalize the inference method to simultaneously account

280  for observations that are of diverse nature, for instance current observations from drifters, pressure from moorings, sea level observations from satellite altimetry. Such extension will require deriving the expected correlation between each of the variable concerned whose feasibility will have to be addressed and will in any case depend on the process modeled.

Moving to more realistic configuration will require evolving the flow synthesis strategy. The present choice allowed to generate flows with arbitrary spatiotemporal structure, even some that are unlikely to occur in the Ocean, in order to enable a broad

285  exploration of the inference performance. Such choice could be pushed further with superpositions of multiple processes, non-separable kernels and will likely require leveraging spectral domain approaches. A switch to flows generated from dynamical models (quasi-geostrophic, primitive equations) may eventually be welcome however to evolve in regimes of variability more closely representative of the actual Ocean dynamics with more realistic representations of process life cycles.

Applications of the inference method to realistic observation datasets (e.g. velocity observations from the Global Drifter

290  Program - Lumpkin et al. (2017)) is also computationally prevented in the present form by the use of dense covariance arrays. Alleviating this constraint will require to leverage sparsity in inference inputs associated from observations that are distant in space and/or time.

*Code availability.*  The software code required to reproduce results are found at the following url: https://github.com/apatlpo/nwa

*Video supplement.*  Animation of the synthetic flow and drifter trajectories in there REF, as well in REG[0.008] and REG[1.6] scenario are

295  provided.

*Author contributions.*  All authors contributed to the conceptualization of this study. A.P., L.A., M.R., A.Z. developed the software required to perform the analysis. A.P. and L.A. conducted the investigation. A.P. produced the visualization. A.P. and L.A. prepared the original manuscript. A.P., L.A., M.R., A.Z. reviewed and edited the manuscript. N.J. and A.P. acquired funding to make this work possible.

*Competing interests.*  The authors declare that they have no conflict of interest.

300  *Acknowledgements.*  A.P. acknowledge support from the Institute of Advanced Studies (University of Western Australian) under the Gledden Visiting Fellowship program, as well as support from the TOSCA-ROSES SWOT project DIEGO. L.A. is supported by the ARC ITRH for Transforming energy Infrastructure through Digital Engineering (TIDE), Grant No. IH200100009.

## Appendix A: MCMC Sampling

### A1    Metropolis-Hastings Algorithm

305    The Metropolis-Hastings algorithm, initially proposed in (Metropolis et al., 1953) and later extended by (Hastings, 2024), generates a proposal $\Theta^{[*]}$ from $\Theta^{[i-1]}$ using some user specified proposal distribution $f(\Theta^{[*]} \mid \Theta^{[i-1]})$. Given a proposal $\Theta^{[*]}$, we accept the sample with probability $r$, where

$$r = \min\left(1, \frac{\mathrm{p}(\Theta^{[*]} \mid \mathbf{y}) f(\Theta^{[i-1]} \mid \Theta^{[*]})}{\mathrm{p}(\Theta^{[i-1]} \mid \mathbf{y}) f(\Theta^{[*]} \mid \Theta^{[i-1]})}\right). \tag{A1}$$

If the proposal density is symmetrical, that is, $f(\Theta^{[i-1]} \mid \Theta^{[*]}) = f(\Theta^{[*]} \mid \Theta^{[i-1]})$, then (A1) reduces to the ratio of the posterior
310    densities and so the MH algorithm will always accept a proposed $\Theta^{[*]}$ that is more probable than $\Theta^{[i-1]}$. The choice of $f(\cdot \mid \cdot)$ is critical to the success of the MH algorithm. If $f(\cdot \mid \cdot)$ is too wide then the algorithm can become stuck for many iterations, thus generating very few unique proposals. Conversely, if $f(\cdot \mid \cdot)$ is too narrow the algorithm will not effectively explore the parameter space, the sampled $\Theta^{[1]}, \ldots, \Theta^{[n]}$ will be highly correlated, and again, few independent samples will be generated. One of the main drawbacks of the MH algorithm is that there are sampling parameters that need to be hand-tuned, we provide
315    some guidance on this in the appendix alongside some diagnostics of the main results.

We parameterise $f(\cdot \mid \cdot)$ as a multivariate normal distribution with mean $\Theta^{[i-1]}$ and diagonal covariance matrix. The standard deviations are set to 1/20th of the true values; this yields an acceptance probability of $\sim 0.25$ which is a widely agreed upon rule-of-thumb to balance exploration and exploitation of the posterior distribution. Full validation results to guarantee fit and convergence of the MCMC estimation algorithm are presented alongside the code at https://github.com/apatlpo/nwa.

320    ### A2    Notes on alternative MCMC sampling algorithms

Modern MCMC algorithms have been dominated by gradient-based proposal methods where a proposal $\Theta^{[*]}$ is generated by assessing the local topology surrounding $\Theta^{[i-1]}$: this allows the algorithm to efficiently trade off notions of exploration and exploitation of the posterior. Included in these algorithms are the popular Hamiltonian Monte Carlo techniques, such as those implemented in Stan (Carpenter et al., 2017), PyMC3 (Salvatier et al., 2016) and Pyro (Bingham et al., 2019); these
325    implementations, as well as others such as GPJax (Pinder and Dodd, 2022) will typically use symbolic toolboxes to define the local topology of the posterior. As discussed above, we parameterise our model using the Matérn covariance function as it exemplifies a number of desirable physical characteristics. However, the derivatives of the Matérn covariance function are difficult to obtain due to $\mathcal{K}_{|\nu|}(\cdot)$: analytical derivatives are only available at integer values of $\nu - 1/2$, and numerical calculations of $\mathcal{K}_{|\nu|}(\cdot)$ are not available in any symbolic toolboxes that we are aware of. Competing MCMC algorithms should not affect
330    the accuracy of the posterior estimation; but rather, they will differ in their sampling efficiency. This study is concerned with inference, and not operationalization, and so we choose the Metropolis-Hastings algorithm so as to avoid the issue of gradients at the cost of some hand-tuning of the algorithm.

# References

Arbic, B. K., Müller, M., Richman, J. G., Shriver, J. F., Morten, A. J., Scott, R. B., Sérazin, G., and Penduff, T.: Geostrophic Turbulence
335   in the Frequency–Wavenumber Domain: Eddy-Driven Low-Frequency Variability, Journal of Physical Oceanography, 44, 2050–2069,
https://doi.org/10.1175/JPO-D-13-054.1, publisher: American Meteorological Society Section: Journal of Physical Oceanography, 2014.

Arbic, B. K., Alford, M. H., Ansong, J. K., Buijsman, M. C., Ciotti, R. B., Farrar, J. T., Hallberg, R. W., Henze, C. E., Hill, C. N.,
Luecke, C. A., Menemenlis, D., Metzger, E. J., Müeller, M., Nelson, A. D., Nelson, B. C., Ngodock, H. E., Ponte, R. M., Rich-
man, J. G., Savage, A. C., Scott, R. B., Shriver, J. F., Simmons, H. L., Souopgui, I., Timko, P. G., Wallcraft, A. J., Zamudio, L.,
340   and Zhao, Z.: A Primer on Global Internal Tide and Internal Gravity Wave Continuum Modeling in HYCOM and MITgcm, in: New
Frontiers in Operational Oceanography, edited by Chassignet, E. P., Pascual, A., Tintoré, J., and Verron, J., GODAE OceanView,
https://doi.org/10.17125/gov2018.ch13, 2018.

Arbic, B. K., Elipot, S., Brasch, J. M., Menemenlis, D., Ponte, A. L., Shriver, J. F., Yu, X., Zaron, E. D., Alford, M. H., Buijsman, M. C., Aber-
nathey, R., Garcia, D., Guan, L., Martin, P. E., and Nelson, A. D.: Near-Surface Oceanic Kinetic Energy Distributions From Drifter Obser-
345   vations and Numerical Models, Journal of Geophysical Research: Oceans, 127, e2022JC018 551, https://doi.org/10.1029/2022JC018551,
2022.

Ballarotta, M., Ubelmann, C., Pujol, M.-I., Taburet, G., Fournier, F., Legeais, J.-F., Faugere, Y., Delepoulle, A., Chelton, D., Dibarboure,
G., and Picot, N.: On the resolutions of ocean altimetry maps, preprint, Operational Oceanography/Sea Level/Surface/All Geographic
Regions, https://doi.org/10.5194/os-2018-156, 2019.

350   Ballarotta, M., Ubelmann, C., Veillard, P., Prandi, P., Etienne, H., Mulet, S., Faugère, Y., Dibarboure, G., Morrow, R., and Picot, N.: Improved
global sea surface height and currents maps from remote sensing and in situ observations, preprint, ESSD – Ocean/Physical oceanography,
https://doi.org/10.5194/essd-2022-181, 2022.

Balwada, D., LaCasce, J. H., and Speer, K. G.: Scale-dependent distribution of kinetic energy from surface drifters
in the Gulf of Mexico, Geophysical Research Letters, 43, 10,856–10,863, https://doi.org/10.1002/2016GL069405, _eprint:
355   https://onlinelibrary.wiley.com/doi/pdf/10.1002/2016GL069405, 2016.

Balwada, D., LaCasce, J. H., Speer, K. G., and Ferrari, R.: Relative Dispersion in the Antarctic Circumpolar Current, Journal of Physical
Oceanography, 51, 553–574, https://doi.org/10.1175/JPO-D-19-0243.1, 2021.

Barth, A., Beckers, J.-M., Troupin, C., Alvera-Azcárate, A., and Vandenbulcke, L.: divand-1.0: $n$-dimensional variational data analysis
for ocean observations, Geoscientific Model Development, 7, 225–241, https://doi.org/10.5194/gmd-7-225-2014, publisher: Copernicus
360   GmbH, 2014.

Barth, A., Troupin, C., Reyes, E., Alvera-Azcárate, A., Beckers, J.-M., and Tintoré, J.: Variational interpolation of high-frequency radar
surface currents using DIVAnd, Ocean Dynamics, 71, 293–308, https://doi.org/10.1007/s10236-020-01432-x, 2021.

Bingham, E., Chen, J. P., Jankowiak, M., Obermeyer, F., Pradhan, N., Karaletsos, T., Singh, R., Szerlip, P., Horsfall, P., and Goodman, N. D.:
Pyro: Deep Universal Probabilistic Programming, Journal of Machine Learning Research, 20, 1–6, http://jmlr.org/papers/v20/18-403.html,
365   2019.

Bretherton, F. P. and McWilliams, J. C.: Estimations from irregular arrays, Reviews of Geophysics, 18, 789–812,
https://doi.org/10.1029/RG018i004p00789, 1980.

Bretherton, F. P., Davis, R. E., and Fandry, C.: A technique for objective analysis and design of oceanographic experiments applied to
MODE-73, Deep Sea Research and Oceanographic Abstracts, 23, 559–582, https://doi.org/10.1016/0011-7471(76)90001-2, 1976.

370    Buckingham, C. E., Naveira Garabato, A. C., Thompson, A. F., Brannigan, L., Lazar, A., Marshall, D. P., George Nurser, A. J., Damerell, G., Heywood, K. J., and Belcher, S. E.: Seasonality of submesoscale flows in the ocean surface boundary layer, Geophysical Research Letters, 43, 2118–2126, https://doi.org/10.1002/2016GL068009, _eprint: https://onlinelibrary.wiley.com/doi/pdf/10.1002/2016GL068009, 2016.

Callies, J. and Ferrari, R.: Interpreting Energy and Tracer Spectra of Upper-Ocean Turbulence in the Submesoscale Range, J. Phys. Oceanogr., 43, 2456–2474, 2013.

375    Callies, J., Barkan, R., and Naveira Garabato, A.: Time scales of submesoscale flow inferred from a mooring array, Journal of Physical Oceanography, 2020.

Carpenter, B., Gelman, A., Hoffman, M. D., Lee, D., Goodrich, B., Betancourt, M., Brubaker, M., Guo, J., Li, P., and Riddell, A.: *Stan* : A Probabilistic Programming Language, Journal of Statistical Software, 76, https://doi.org/10.18637/jss.v076.i01, 2017.

D'Asaro, E. A., Shcherbina, A. Y., Klymak, J. M., Molemaker, J., Novelli, G., Guigand, C. M., Haza, A. C., Haus, B. K., Ryan, E. H., Jacobs,
380    G. A., and others: Ocean convergence and the dispersion of flotsam, Proceedings of the National Academy of Sciences, 115, 1162–1167, publisher: National Acad Sciences, 2018.

De Marez, C., Callies, J., Haines, B., Rodriguez-Chavez, D., and Wang, J.: Observational Constraints on the Submesoscale Sea Surface Height Variance of Balanced Motion, Journal of Physical Oceanography, 53, 1221–1235, https://doi.org/10.1175/JPO-D-22-0188.1, 2023.

Delandmeter, P. and van Sebille, E.: The Parcels v2.0 Lagrangian framework: new field interpolation schemes, Geoscientific Model Devel-
385    opment, 12, 3571–3584, https://doi.org/10.5194/gmd-12-3571-2019, publisher: Copernicus GmbH, 2019.

Elipot, S., Lumpkin, R., and Prieto, G.: Modification of inertial oscillations by the mesoscale eddy field, Journal of Geophysical Research: Oceans, 115, publisher: Wiley Online Library, 2010.

Elipot, S., Lumpkin, R., Perez, R. C., Lilly, J. M., Early, J. J., and Sykulski, A. M.: A global surface drifter data set at hourly resolution, Journal of Geophysical Research: Oceans, 121, 2937–2966, https://doi.org/10.1002/2016JC011716, 2016.

390    Farrar, J. T., D'Asaro, E., Rodriguez, E., Shcherbina, A., Czech, E., Matthias, P., Nicholas, S., Bingham, F., Mahedevan, A., Omand, M., Rainville, L., Lee, C., Chelton, D., Samelson, R., O'Neill, L., Lenain, L., Menemenlis, D., Perkovic-Martin, D., Mouroulis, P., Gierach, M., Thompson, D., Wineteer, A., Torres, H., Klein, P., Thompson, A., McWilliams, J. C., Molemaker, J., Barkan, R., Wenegrat, J., Rocha, C., Jacobs, G., D'Addezio, J., de Halleux, S., and Jenkins, R.: S-MODE: The Sub-Mesoscale Ocean Dy- namics Experiment, in: IGARSS 2020 - 2020 IEEE International Geoscience and Remote Sensing Symposium, pp. 3533–3536,
395    https://doi.org/10.1109/IGARSS39084.2020.9323112, iSSN: 2153-7003, 2020.

Ferrari, R. and Wunsch, C.: Ocean Circulation Kinetic Energy: Reservoirs, Sources, and Sinks, Annual Review of Fluid Mechanics, 41, 253–282, 2009.

Freeland, H., Rhines, P., and Rossby, T.: Statistical observations of the trajectories of neutrally buoyant floats in the North Atlantic, Journal of Marine Research, 33, https://elischolar.library.yale.edu/journal_of_marine_research/1327, 1975.

400    Hastings, W. K.: Monte Carlo Sampling Methods Using Markov Chains and Their Applications, 2024.

Jones, C. S., Xiao, Q., Abernathey, R. P., and Smith, K. S.: Using Lagrangian Filtering to Remove Waves From the Ocean Surface Ve- locity Field, Journal of Advances in Modeling Earth Systems, 15, e2022MS003 220, https://doi.org/10.1029/2022MS003220, _eprint: https://onlinelibrary.wiley.com/doi/pdf/10.1029/2022MS003220, 2023.

Lilly, J. M. and Gascard, J.-C.: Wavelet ridge diagnosis of time-varying elliptical signals with application to an oceanic eddy, Nonlinear
405    Processes in Geophysics, 13, 467–483, https://doi.org/10.5194/npg-13-467-2006, 2006.

Lilly, J. M., Scott, R. K., and Olhede, S. C.: Extracting waves and vortices from Lagrangian trajectories, Geophysical Research Letters, 38, n/a–n/a, https://doi.org/10.1029/2011GL049727, 2011.

Lilly, J. M., Sykulski, A. M., Early, J. J., and Olhede, S. C.: Fractional Brownian motion, the Matérn process, and stochastic modeling of turbulent dispersion, Nonlinear Processes in Geophysics, 24, 481–514, https://doi.org/10.5194/npg-24-481-2017, 2017.

410 Lumpkin, R., Treguier, A.-M., and Speer, K.: Lagrangian Eddy Scales in the Northern Atlantic Ocean, JOURNAL OF PHYSICAL OCEANOGRAPHY, 32, 2002.

Lumpkin, R., Özgökmen, T., and Centurioni, L.: Advances in the application of surface drifters, Annual Review of Marine Science, 9, 59–81, publisher: Annual Reviews, 2017.

Metropolis, N., Rosenbluth, A. W., Rosenbluth, M. N., Teller, A. H., and Teller, E.: Equation of State Calculations by Fast Computing

415 Machines, The Journal of Chemical Physics, 21, 1087–1092, https://doi.org/10.1063/1.1699114, 1953.

Middleton, J. F.: Drifter spectra and diffusivities, Journal of Marine Research, 43, 37–55, 1985.

Morrow, R., Fu, L.-L., Ardhuin, F., Benkiran, M., Chapron, B., Cosme, E., d'Ovidio, F., Farrar, J. T., Gille, S. T., Lapeyre, G., Le Traon, P.-Y., Pascual, A., Ponte, A., Qiu, B., Rascle, N., Ubelmann, C., Wang, J., and Zaron, E. D.: Global Observations of Fine-Scale Ocean Surface Topography With the Surface Water and Ocean Topography (SWOT) Mission, Frontiers in Marine Science, 6, 232,

420 https://doi.org/10.3389/fmars.2019.00232, 2019.

Pearson, J., Fox-Kemper, B., Barkan, R., Choi, J., Bracco, A., and McWilliams, J. C.: Impacts of Convergence on Structure Functions from Surface Drifters in the Gulf of Mexico, Journal of Physical Oceanography, 49, 675–690, https://doi.org/10.1175/JPO-D-18-0029.1, 2019.

Pearson, J., Fox-Kemper, B., Pearson, B., Chang, H., Haus, B. K., Horstmann, J., Huntley, H. S., Kirwan, A. D., Lund, B., and Poje, A.: Biases in Structure Functions from Observations of Submesoscale Flows, Journal of Geophysical Research: Oceans, 125, e2019JC015 769,

425 https://doi.org/10.1029/2019JC015769, 2020.

Pinder, T. and Dodd, D.: GPJax: A Gaussian Process Framework in JAX, Journal of Open Source Software, 7, 4455, https://doi.org/10.21105/joss.04455, 2022.

Poje, A. C., Ozgokmen, T. M., Lipphardt, B. L., Haus, B. K., Ryan, E. H., Haza, A. C., Jacobs, G. A., Reniers, A. J. H. M., Olascoaga, M. J., Novelli, G., Griffa, A., Beron-Vera, F. J., Chen, S. S., Coelho, E., Hogan, P. J., Kirwan, A. D., Huntley, H. S., and Mariano,

430 A. J.: Submesoscale dispersion in the vicinity of the Deepwater Horizon spill, Proceedings of the National Academy of Sciences, 111, 12 693–12 698, https://doi.org/10.1073/pnas.1402452111, 2014.

Poje, A. C., Özgökmen, T. M., Bogucki, D. J., and Kirwan, J. A. D.: Evidence of a forward energy cascade and Kolmogorov self-similarity in submesoscale ocean surface drifter observations, Physics of Fluids, 29, 020 701, https://doi.org/10.1063/1.4974331, 2017.

Polzin, K. L. and Lvov, Y. V.: Toward regional characterizations of the oceanic internal wavefield, Reviews of Geophysics, 49, 2011.

435 Pujol, M.-I., Faugère, Y., Taburet, G., Dupuy, S., Pelloquin, C., Ablain, M., and Picot, N.: DUACS DT2014: the new multi-mission altimeter data set reprocessed over 20 years, Ocean Science, 12, 1067–1090, https://doi.org/10.5194/os-12-1067-2016, publisher: Copernicus GmbH, 2016.

Qiu, B., Chen, S., Klein, P., Wang, J., Torres, H., Fu, L.-L., and Menemenlis, D.: Seasonality in Transition Scale from Balanced to Unbalanced Motions in the World Ocean, Journal of Physical Oceanography, 48, 591–605, https://doi.org/10.1175/JPO-D-17-0169.1, 2018.

440 Salvatier, J., Wiecki, T. V., and Fonnesbeck, C.: Probabilistic programming in Python using PyMC3, PeerJ Computer Science, 2, e55, https://doi.org/10.7717/peerj-cs.55, 2016.

Shcherbina, A. Y., Sundermeyer, M. A., Kunze, E., D'Asaro, E., Badin, G., Birch, D., Brunner-Suzuki, A.-M. E., Callies, J., Kuebel Cervantes, B. T., Claret, M., and others: The LatMix summer campaign: Submesoscale stirring in the upper ocean, Bulletin of the American Meteorological Society, 96, 1257–1279, 2015.

445    Sykulski, A. M., Olhede, S. C., Lilly, J. M., and Danioux, E.: Lagrangian Time Series Models for Ocean Surface Drifter Trajectories, Journal of the Royal Statistical Society Series C: Applied Statistics, 65, 29–50, https://doi.org/10.1111/rssc.12112, 2016.

Torres, H., Klein, P., Siegelman, L., Qiu, B., Chen, S., Ubelmann, C., Wang, J., Menemenlis, D., and Fu, L.-L.: Diagnosing ocean-wave-turbulence interactions from space, Geophysical Research Letters, 46, 8933–8942, publisher: Wiley Online Library, 2019.

Ubelmann, C., Dibarboure, G., Gaultier, L., Ponte, A., Ardhuin, F., Ballarotta, M., and Faugère, Y.: Reconstructing Ocean Surface Cur-
450    rent Combining Altimetry and Future Spaceborne Doppler Data, Journal of Geophysical Research: Oceans, 126, e2020JC016 560, https://doi.org/10.1029/2020JC016560, 2021.

Ubelmann, C., Carrere, L., Durand, C., Dibarboure, G., Faugère, Y., Ballarotta, M., Briol, F., and Lyard, F.: Simultaneous estimation of ocean mesoscale and coherent internal tide sea surface height signatures from the global altimetry record, Ocean Science, 18, 469–481, https://doi.org/10.5194/os-18-469-2022, publisher: Copernicus GmbH, 2022.

455    Veneziani, M., Griffa, A., Reynolds, A. M., and Mariano, A. J.: Oceanic Turbulence and Stochastic Models from Subsurface La-grangian Data for the Northwest Atlantic Ocean, Journal of Physical Oceanography, 34, 1884–1906, https://doi.org/10.1175/1520-0485(2004)034<1884:OTASMF>2.0.CO;2, 2004.

Wang, H. and Bühler, O.: Anisotropic Statistics of Lagrangian Structure Functions and Helmholtz Decomposition, JOURNAL OF PHYSI-CAL OCEANOGRAPHY, 51, 2021.

460    Wortham, C. and Wunsch, C.: A Multidimensional Spectral Description of Ocean Variability, Journal of Physical Oceanography, 44, 944–966, https://doi.org/10.1175/JPO-D-13-0113.1, 2014.

Wunsch, C.: Toward a Midlatitude Ocean Frequency–Wavenumber Spectral Density and Trend Determination, Journal of Physical Oceanog-raphy, 40, 2264–2281, https://doi.org/10.1175/2010JPO4376.1, publisher: American Meteorological Society Section: Journal of Physical Oceanography, 2010.

465    Yu, X., Naveira Garabato, A. C., Martin, A. P., Buckingham, C. E., Brannigan, L., and Su, Z.: An Annual Cycle of Submesoscale Vertical Flow and Restratification in the Upper Ocean, Journal of Physical Oceanography, 49, 1439–1461, https://doi.org/10.1175/JPO-D-18-0253.1, 2019a.

Yu, X., Ponte, A. L., Elipot, S., Menemenlis, D., Zaron, E. D., and Abernathey, R.: Surface Kinetic Energy Distributions in the Global Oceans From a High-Resolution Numerical Model and Surface Drifter Observations, Geophysical Research Letters, 46, 9757–9766,
470    https://doi.org/10.1029/2019GL083074, 2019b.

Zang, X. and Wunsch, C.: Spectral Description of Low-Frequency Oceanic Variability, Journal of Physical Oceanography, 31, 3073–3095, https://doi.org/10.1175/1520-0485(2001)031<3073:SDOLFO>2.0.CO;2, publisher: American Meteorological Society Section: Journal of Physical Oceanography, 2001.

Zhang, H., Prater, M. D., and Rossby, T.: Isopycnal Lagrangian statistics from the North Atlantic Current RAFOS float observations, Journal
475    of Geophysical Research: Oceans, 106, 13 817–13 836, https://doi.org/10.1029/1999JC000101, 2001.